JOURNAL OF SOLID STATE CHEMISTRY 113, 62–73 (1994)

Phase Equilibria and Structural Studies on the Solid Solution $MgTi_2O_5$–Ti_3O_5

I. E. Grey, C. Li, and I. C. Madsen

CSIRO Division of Mineral Products, P.O. Box 124, Port Melbourne, Victoria 3207, Australia

Received August 5, 1993; in revised form January 28, 1994; accepted January 31, 1994

Phase equilibria involving the pseudobrookite-type solid solution series $Mg_{1-x}Ti_{2+x}O_5$, $0.1 < x < 1$, were determined as a function of oxygen fugacity at 1473 K. The quenching method was used and oxygen fugacities in the range 10^{-14}–10^{-19} atm were obtained using H_2/CO_2 and H_2/H_2O mixtures. Members of the solid solution have orthorhombic symmetry for $x < 0.72$ and monoclinic symmetry for $x > 0.72$. From Rietveld refinements, the origin of the symmetry lowering was found to be Ti^{3+}–Ti^{3+} bonding in the *M*2 sites. *M*2–*M*2 is constant at 2.92 Å in the orthorhombic phases and decreases monotonically in the monoclinic phases to a value of 2.74 Å at $x = 1$. The solid solution members were found to be nonstoichiometric with the oxygen to metal atomic ratio, [O]/[*M*], higher than the stoichiometric value of 1.667. The [O]/[*M*] ratio has a maximum value of 1.705 near the orthorhombic to monoclinic transition. Constrained site occupation refinements gave (Mg in *M*1)/ΣMg = 0.6 at $x = 0$ and increasing with increasing x to 1.0, corresponding to full ordering, at $x = 0.9$. An alternative interpretation of the results was considered: the *apparent* Mg ordering obtained in the refinements was compensating for ordering of cation vacancies in *M*1. On this basis, and assuming that the Mg ordering had the same dependency on x as for the corresponding $Fe_{1-x}Ti_{2+x}O_5$ solid solution, site occupancy refinements led to calculated values of [O]/[*M*] that agreed with the experimental values obtained from analyses.

INTRODUCTION

Pseudobrookite-type (1) M_3O_5 solid solutions containing $MgTi_2O_5$ and Ti_3O_5 as principal components, together with $FeTi_2O_5$ and Al_2TiO_5, form the dominant phase in high-titania slags produced by electrosmelting of ilmenite (2). The slags are used as feedstocks for titania pigment production by the sulphate process (3), which accounts for half of the 3 million tonnes of pigment produced annually. Addition of MgO during reduction of ilmenite, to stabilise an acid-soluble M_3O_5 phase, has also been proposed as a means of producing a sulfate-route feedstock at subslagging temperatures (4). There is therefore considerable interest in the preparation and properties of the M_3O_5 solid solutions.

The solid solution between $MgTi_2O_5$ and Ti_3O_5, $Mg_{1-x}Ti_{2+x}O_5$, was investigated at slagging temperatures (1823 and 1923 K) by Tuset (5) as part of a study of the system $MgTiO_3$–TiO_2–Ti_2O_3. The samples were equilibrated in controlled gaseous atmospheres (H_2/H_2O mixtures) and cooled in argon or quenched in water. The solid solution was found to be discontinuous at 1823 K, with a miscibility gap extending from $x = 0.88$ to $x = 0.94$. A change in the symmetry from orthorhombic to monoclinic was observed for compositions with x greater than 0.66. $MgTi_2O_5$ showed no observable deviation from stoichiometry. However, with increasing Ti_3O_5 content the solid solution displayed increasing nonstoichiometry, toward higher [O]/[Ti] ratios. The range of [O]/[Ti] found for $Ti_3O_{5+\delta}$ at 1823 K was 1.66–1.70.

Borowiec and Rosenqvist reported results on the stability field of the $Mg_{1-x}Ti_{2+x}O_5$ solid solution as part of a broader study on the system Fe–Ti–Mg–O (6). Their equilibrations, at temperatures in the range 1173–1373 K, were carried out in sealed evacuated silica tubes. A phase diagram was presented for the subsystem TiO–TiO_2–MgO at 1323 K which showed a miscibility gap in the M_3O_5 solid solution extending from $x = 0.85$ to $x = 0.95$. Within this composition range the monoclinic form of Ti_3O_5 (7), containing 1.7 mole% MgO, coexisted with the orthorhombic, pseudobrookite form of M_3O_5, containing 5 mole% MgO. At high Ti_3O_5 contents the M_3O_5 compositions extended towards the *MO* components, giving nonstoichiometric phases with [O]/[*M*] < 1.667, in contrast to the oxygen-excess compositions found at higher temperatures by Tuset (5). For example at $x = 0.85$ the composition range, as measured off Fig. 13 in Ref. (6), was $1.60 < [O]/[M] < 1.66$. For the titanium end-member the single phase composition range was for $1.63 < [O]/[M] < 1.69$ (6). From their broader study of the Fe_2TiO_5–$MgTi_2O_5$–Ti_3O_5 system, Borowiec and Rosenqvist concluded that the solid solution was oxygen deficient, $M_3O_{5-\delta}$, for all ternary compositions with a molar ratio Ti_3O_5/Fe_2TiO_5 greater than 2.

Teller *et al.* (8) characterised four M_3O_5 compositions containing both magnesium and iron by Rietveld refinement of neutron data and Mössbauer spectroscopy. Two

0022-4596/94 $6.00

of the compositions were essentially single phase slags produced by electrosmelting of ilmenite at > 1973 K. One composition, with $x = 0.36$, was stoichiometric whereas the other, with higher $x = 0.52$, was nonstoichiometric with $[O]/[M] = 1.72$. The structure refinement showed that the nonstoichiometry was due to cation vacancies that were localized at the $M1$ sites (fourfold sites in the orthorhombic structure).

The most recently reported study of the system $MgTi_2O_5$–Ti_3O_5 is by Steinbruck and Feltz (9). They prepared solid solution members by reacting mixtures of $MgTi_2O_5$, TiO_2, and Ti_2O_3 in gettered argon at 1573 K. The oxidation state of titanium in the single-phase reaction products was checked by coulometric titration and found to agree within the experimental error with that calculated for the stoichiometric compositions. Steinbruck and Feltz measured the electrical and magnetic properties of solid solution members. They found a large drop in the activation energy for electrical conductivity at an x value between 0.5 and 0.7 which they attributed to Ti–Ti pair formation at the higher Ti^{3+} concentrations.

As part of a general study on phase equilibria and crystal chemistry of M_3O_5 solid solutions incorporating Ti_3O_5 (10, 11) we carried out controlled gaseous atmosphere equilibration studies on the solid solution $MgTi_2O_5$–Ti_3O_5 at 1473 K, supplemented with sealed silica tube studies at 1323K. In view of the contrasting results obtained by different authors on the nonstoichiometry in this system as described above, we paid particular attention to this aspect of the study. The phase studies were supplemented with Rietveld refinements of the powder X-ray diffraction patterns of single phase compositions to gain an understanding of the structural origins of the deviations from stoichiometry. The results of the phase equilibria and powder XRD studies are reported here.

EXPERIMENTAL

Controlled Atmosphere Studies

Starting materials for the equilibration studies were Fisher certified, anatase form TiO_2 and analytical reagent grade MgO. The titania was dried at 1073 K before use and the magnesia was heated to constant weight at 1073 K to determine the amount of adsorbed water and carbon dioxide. An appropriate correction was made when making mixtures of the two components. Weighed mixtures of the two powder samples were thoroughly mixed and pressed into 1-cm-diameter pellets. A number of pellets with different [Mg]/[Mg + Ti] atomic ratios were placed in separate compartments of a boat made from molybdenum metal sheet, and simultaneously equilibrated in a flowing gaseous atmosphere in a horizontal tube furnace. At the end of the equilibration period the samples were rapidly cooled by withdrawing the boat to a brass quench-end (12). To obtain equilibrium products it was necessary to regrind and reheat at least once. Most samples underwent two or more reheats for periods of typically 20–70 hr. Oxygen fugacity cycling was also used to ensure that equilibrium was achieved.

For oxygen fugacities higher than 10^{-16} atm at 1473 K, the controlled gaseous atmospheres were obtained using H_2/CO_2 mixtures. For oxygen fugacities lower than 10^{-16} atm, more accurate control of the gas ratios and avoidance of carbon deposition was achieved using H_2/H_2O mixtures in a two-stage gas control system. In the first stage hydrogen was saturated with water vapor at 273 K. The H_2/H_2O mixture was then mixed with high purity hydrogen in a second stage. H_2/H_2O ratios up to $10^4:1$ could be obtained by this method. It was necessary to increase the reaction time to allow for the very low rate of oxygen exchange when the high ratios were used.

The oxygen content of the pellets was determined from the weight gain on oxidation to mixtures of TiO_2 and $MgTi_2O_5$ at 1173 K. The [Mg]/[Mg + Ti] ratio for selected samples was checked by quantitative energy dispersive analyses using a scanning electron microscope. The range of oxygen fugacities studied was 10^{-14}–10^{-19} atm. Further details of the apparatus used and the procedure are given in Ref. (12), and a discussion of experimental errors is given in Ref. (11).

For the determination of the phase boundaries of the M_3O_5 phase, XRD was used to detect the first appearance of a second phase, M_2O_3 or reduced rutile, MO_{2-x}. In the case of the reduced rutile phase boundaries, the level of incorporation of MgO was very low and the appearance of M_3O_5 as a second phase did not give a precise location of the reduced rutile phase boundary. The procedure used in this case was to equilibrate a number of pellets with [Mg]/[Mg + Ti] ratios higher than that at the boundary. The height of the (101) diffraction peak of the minor M_3O_5 phase was measured in the XRD patterns of each of the two-phase products. The plots of peak height versus [Mg]/[Mg + Ti] were linear, and extrapolation to zero peak height gave the boundary composition for the reduced rutile phase.

Sealed Silica Tube Studies

The determination of the nonstoichiometry range for Ti_3O_5 at 1323 K made use of the transport of oxygen between oxide pellets in a temperature gradient. The principle of the method is shown schematically in Fig. 1. Up to nine small pellets with identical compositions close to Ti_3O_5, made from mixtures of TiO_2 and Ti_2O_3, were sealed in an evacuated silica tube and placed in a temperature gradient of 1323–1313 K over the 6-cm tube length. The tube was held at temperature for 60 hr, during which time oxygen transport occurred from pellets at the hotter end

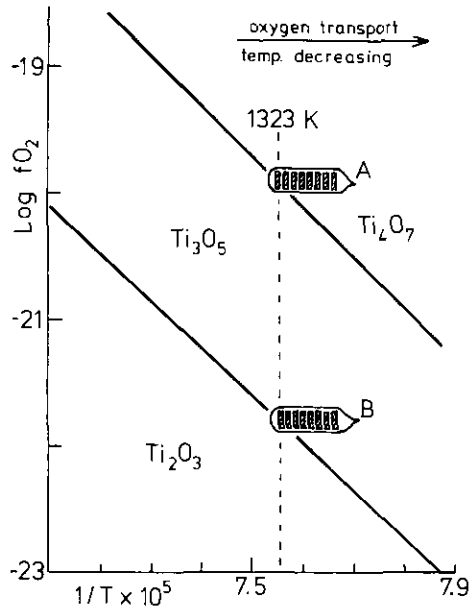

FIG. 1. Stoichiometry determination by inter-pellet oxygen transfer in a sealed evacuated tube in a temperature gradient. Pellets in tubes A and B have starting compositions with $1.67 < [O]/[Ti] <$ and $1.50 < [O]/[Ti] < 1.667$, respectively.

to pellets at the cooler end. The tube was quenched in liquid nitrogen and the phases in each of the pellets identified by XRD. Depending on the starting composition, the pellets comprised Ti_3O_5 with different amounts of either Ti_2O_3 or Ti_4O_7. Pellets which contained the smallest trace of a second phase were oxidised to constant weight at 1273 K to determine the oxygen content at the limits of the nonstoichiometry range of Ti_3O_5.

Rietveld Refinements

X-ray intensity data on micronized single phase M_3O_5 samples were collected on a Philips diffractometer fitted with a graphite monochromator in the diffracted beam and employing Cu$K\alpha$ radiation. Step-scan intensity measurements in the 2θ range 16–140° were made at intervals of 0.025°. A variable step-counting time strategy (13) was used that increases the counting time with diffraction angle in a manner inversely proportional to the intensity fall-off from factors such as Lorentz-polarization, form factor and thermal parameters. This results in a relatively uniform intensity distribution over the whole angular range. The total counting time was typically 30,000 sec. The X-ray tube was operated at 40 kV and 40 mA, with a 1° divergence slit, a 0.2-mm receiving slit, a 1° scatter slit, and soller slits.

Least-squares structure refinements were carried out using the Rietveld program RIET7, a local modification of the code by Hill and Howard (14) and Wiles and Young (15) which takes account of variable-time data sets. Profile refinement parameters included a scale factor, a pseudo-Voigt peak shape parameter, a peak full-width at half maximum (FWHM) function (16) of the form $FWHM^2 = U\tan^2\theta + V\tan\theta + W$, where U, V, and W are refinable parameters which were calculated for seven half-widths on either side of the peak maximum, a 2θ zero parameter and the unit cell parameters. The background was refined using a four-parameter polynomial in $2\theta^n$ where n has values from 0 to 3 inclusive. An experimentally determined value of 0.91 was used for the monochromator polarisation correction (17). X-ray scattering factors for both ionized and neutral atoms, including anomalous dispersion, were taken from the "International Tables for X-Ray Crystallography" (18).

Refinements were initiated using the reported atomic coordinates for pseudobrookite (1), high-Ti_3O_5 (19) and low-Ti_3O_5 (7) as starting coordinates for the orthorhombic, high-monoclinic (H) and low-monoclinic (M) structures respectively. *Ccmm* was used as the space group setting for the orthorhombic phases to maintain the same cell parameter sequence as for the monoclinic phases with space group C2/m, i.e., $a \sim 9.8$, $b \sim 3.8$, $c \sim 9.9$ Å. Refinement of the end member compositions $MgTi_2O_5$ and Ti_3O_5 (both low and high forms) was hampered due to preferred orientation. This was minimised by grinding the samples in a McCrone micronizing mill and back loading them onto a textured paper surface. A correction was still necessary, and a number of refinements were carried out using different preferred orientation planes. The refinement program uses the March model for preferred orientation, as implemented by Dollase (20). The lowest Bragg R-factor was obtained using [010] as the scattering vector for $MgTi_2O_5$ and [001] for Ti_3O_5. The sign of the refined orientation factor was of opposite sign for the two cases, consistent with a lath or needle [010] habit for the former and a (001) plate-like habit for the latter. The two different habits were confirmed by optical microscopy. The solid solution members had less well developed morphologies and the preferred orientation effects were very small.

RESULTS AND DISCUSSION

Phase Equilibria

The results of the controlled equilibrations at 1473 K are presented in Fig. 2 as a plot of log fO_2 vs [Mg]/[Mg + Ti] atomic ratio. The stability field for the M_3O_5 solid solution is delineated in Fig. 2, as well as the phase boundaries for those phases that coexist with M_3O_5. These are the M_2O_3 solid solution ($MgTiO_3$–Ti_2O_3) and the reduced rutile phases. The incorporation of Mg into the reduced rutile phases was found to be very low; typically the limiting [Mg]/[Mg + Ti] ratio was less than 0.005, corresponding to less than 0.3 wt% MgO. Borowiec and

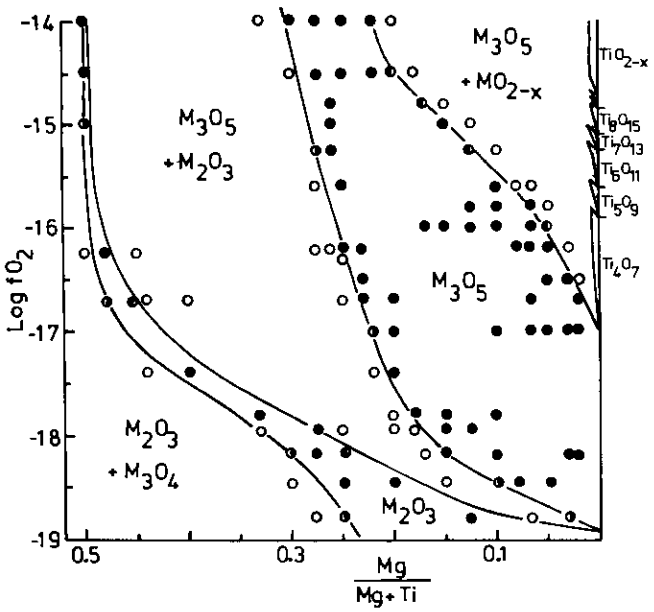

FIG. 2. Oxygen fugacity versus composition for the Mg–Ti–O system at 1473 K, for $10^{-14} < fO_2 < 10^{-19}$ atm. Experimental data: filled circles, single phase; open circles, two phases; and half-filled circles, trace of second phase.

Rosenqvist (6) reported MgO contents of less than 0.1 wt% in reduced rutile phases coexisting with M_3O_5 at a temperature of 1373 K, while at a temperature of 1823 K Tuset (5) reported limiting MgO contents in the range 0.8–2.5 wt% for reduced rutile phases having [O]/[M] ratios in the range 1.8 to 2.0.

From Fig. 2, the M_2O_3 solid solution phases are seen to exist over narrow fO_2 ranges. For $Mg_{1-y}Ti_{1+y}O_3$ compositions with $0.1 < y < 0.5$, the oxygen fugacity range separating $M_2O_3 + M_3O_4$ from $M_2O_3 + M_3O_5$ is less than 0.5 log fO_2 units. This is consistent with the presence of a large region of immiscibility in the M_2O_3 solid solution at lower temperatures (6). According to the recent study of the $MgTiO_3$–Ti_2O_3 system by Sheikh and Irvine (21), the immiscibility dome closes at a temperature just below 1273 K. From XRD studies on samples quenched from various temperatures, they established a first-order phase transition from $MgTiO_3$ (ordered $R\bar{3}$ ilmenite-type structure) to Ti_2O_3 (disordered $R\bar{3}c$ corundum-type structure) at a boundary that intercepted the solvus at close to $y = 0.5$, $t = 1073$ K, and moved to lower y values with increasing temperature. According to Sheikh and Irvine's (21) phase diagram (Fig. 4 in Ref. (21)), samples quenched from the temperature of our study, 1473 K, should comprise a corundum-type phase for all values of y. In practice, we observed sharp cation-ordering reflections due to the ordered ilmenite-type structure in the XRD patterns for y less than about 0.1. For $0.1 < y < 0.5$ the cation-ordering reflections became progressively broader and weaker, while for $y > 0.5$ the XRD peaks corresponded to the disordered corundum-type phase only. Evidently the cation diffusions are fast enough to establish domains of the ordered structure measuring some 100's of angstroms during the rapid cooling (of the order of 100 K sec^{-1}) used in our study.

For the oxygen fugacity range used in our study, 10^{-14}–10^{-19} atm, the $Mg_{1-x}Ti_{2+x}O_5$ solid solution extends from $x = 0.1$ to $x = 1$. The end member composition with $x = 0$ was also prepared, by reaction in air, to provide a sample for structure refinement. For compositions with $x < 0.7$ the XRD patterns were indexed with an orthorhombic pseudobrookite-type cell. At $x = 0.76$, splitting of certain XRD peaks due to a monoclinic distortion was discernible. The monoclinic distortion increased with increasing x, to a maximum β angle of 91.26° at $x = 1$. A plot of β vs x gave the transition from orthorhombic to monoclinic symmetry at $x = 0.72$. The XRD patterns for compositions with $x > 0.94$ comprised peaks due to two monoclinic phases, corresponding to the high- and low-temperature forms of Ti_3O_5 (7). The high- to low-temperature reversible reaction occurs at 448 K in pure Ti_3O_5 (22). The coexistence of the two phases in rapidly cooled samples may reflect a discontinuity in the solid solution, as reported by Tuset (5) from studies at 1823 K. Alternatively the results can be interpreted in terms of incomplete conversion of the high- to the low-temperature form on cooling, the kinetics of which become more sluggish as the amount of MgO substituting into Ti_3O_5 increases. The relative amounts of the low- and high-temperature forms varied in different equilibrations of the same composition. This is interpreted to be due to small local fluctuations in the [Mg]/[Mg + Ti] ratio within the sample. A more extreme representation of this effect was the coexistence of orthorhombic and monoclinic M_3O_5 phases in quenched products from single equilibrations of compositions with $x > 0.7$. Regrinding and reequilibrating resulted in single-phase monoclinic M_3O_5. This type of small-scale inhomogeneity in the MgO distribution may explain the miscibility gap in the range $0.85 < x < 0.95$ at 1323 K reported by Borowiec and Rosenqvist (6), where a single equilibration was employed.

Nonstoichiometry in M_3O_5

Figure 2 gives no information on the oxygen content of the solid solution phases. This was obtained from the weight gain on oxidation to mixtures of $MgTi_2O_5$ and TiO_2. The results are plotted as [O]/[M] atomic ratio vs x in Fig. 3. The filled circles correspond to phases equilibrated at fO_2 values close to the upper ($M_3O_5 + MO_{2-x}$) phase boundary, while the open circles correspond to equilibrations at fO_2 values close to the lower ($M_3O_5 + M_2O_3$) phase boundary. The [O]/[M] ratios are higher than the

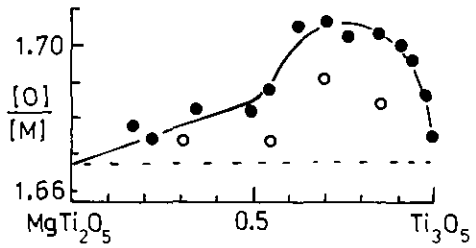

FIG. 3. [O]/[M] atomic ratio vs x for $Mg_{1-x}Ti_{2+x}O_5$. Filled and open circles represent samples equilibrated close to the upper (M_3O_5 + MO_{2-x}) and lower (M_3O_5 + M_2O_3) phase boundaries, respectively.

stoichiometric value of 5/3 = 1.667. The nonstoichiometry increases with increasing x to a broad maximum value of [O]/[M] of 1.705 centred at $x \sim 0.75$ for phases equilibrated near the upper phase boundary. For $x > 0.85$ the nonstoichiometry progressively decreases towards a value of 1.675 for the titanium end member. The [O]/[M] ratios in phases equilibrated close to the lower boundary are closer to the stoichiometric value. These results are in general agreement with those obtained by Tuset (5), who also employed equilibration in controlled gaseous atmospheres, at the higher temperature of 1823 K. In contrast, Borowiec and Rosenqvist (6), who equilibrated their samples in sealed evacuated silica tubes at 1323 K, obtained [O]/[M] ratios lower than the stoichiometric value. The results of our sealed silica tube experiments at 1323 K for Ti_3O_5 are given in Table 1. At this lower temperature the nonstoichiometry range is seen to be very narrow, with deviations of no more than 0.002 in the [O]/[Ti] ratio.

In an attempt to glean further information on the nonstoichiometry, structure refinements were undertaken for single-phase M_3O_5 samples. Given that the essential features of the pseudobrookite structure are maintained, the observed high [O]/[M] ratios may be due to either extra anions occupying cavities in the structure or to cation vacancies. The latter is the more usual way of accomodating positive deviations from stoichiometric [O]/[M] ratios in close-packed oxides. Cation vacancies were recently reported in M_3O_5 from a titania slag produced at very high temperatures (8). However, the M_3O_5 structures are relatively open structures with large cavities and so the possibility of excess oxygen cannot be ruled out. An examination of the pseudobrookite structure shows that cavities centred at ~(0.525, 0, 1/4) are surrounded by nine oxygen atoms at distances in the range 2.4–2.9 Å plus two oxygen atoms at 3.8 Å. Clearly, only small relaxations of the surrounding oxygen atoms are needed to provide a suitably sized site for an extra oxygen atom.

TABLE 1
Determination of Stoichiometry Range of Ti_3O_5 at 1323 K

Pellet no.	Starting [O]/Ti]	Phases present (by XRD)	Measured [O]/[Ti]
1–5	1.650	Ti_3[a] + Ti_2 (decreasing 1 to 5)	
6		Ti_3 + Ti_2 (trace)	1.663
7–9		Ti_3	1.665
1–4	1.685	Ti_3	1.666
5		Ti_3 + Ti_4 (trace)	1.668
6		Ti_3 + Ti_4 (minor)	
7		Ti_4 + Ti_3 (trace)	
8–9		Ti_4	1.748

[a] Ti_n an abbreviation for Ti_nO_{2n-1}.

Difference Fourier maps were used to check for the presence of interstitial oxygen. No evidence was found for extra scattering matter in the cavity regions. The maximum measured [O]/[M] ratio of 1.705 corresponds to ~0.5 excess oxygen per unit cell. If it was confined to a fourfold site, (x 0 1/4), at the cavity centre, this represents only 1/8 oxygen per site or 1 electron, which would be at the limit of detection in a Fourier map produced from powder data. Attempts to incorporate a partially occupied cavity site into the Rietveld refinements resulted in significant deteriorations in the fit parameters when the scattering was increased above about 1/16 oxygen per site. The results, although not conclusive, do not support excess oxygen in the structure.

Checking for the presence of cation vacancies also presents formidable difficulties, both because of the small changes in cation site scattering involved ($MO_{1.70}$ = $M_{2.98}\square_{0.02}O_5$), and because of the unknown distribution of the low atomic number element magnesium over the cation sites. It was anticipated that a refinement of the average scattering in the two independent metal atom sites, $M1$ and $M2$, coupled with results on the bulk [Mg]/[Mg + Ti] ratio and bond length–bond strength relationships would provide the required information on the presence and distribution of cation site vacancies. To check the validity of this approach an initial series of refinements was carried out to measure the sensitivity of the refined occupancy of sites $M1$ and $M2$ to various factors (23). The data for $MgTi_2O_5$, which has the smallest deviation from stoichiometry, was used. Unconstrained refinement of the Mg to Ti ratio was allowed in both sites.

It was found that preferred orientation had no significant effect on the refined site occupancies (23). However the ionisation state of the atoms had a profound effect. The average refined metal atom scattering was 17.3 electrons when neutral atoms were used and 19.8 electrons when fully ionized atoms, Mg^{2+}, Ti^{4+}, O^{2-}, were used, cf. 18.7 electrons for $Mg_{0.33}Ti_{0.67}$ and 18.3 electrons for $(Mg_{0.33}Ti_{0.67})_{0.98}\square_{0.02}$. Clearly the effect due to cation vacancies would be completely swamped by errors introduced in the choice of ionisation states. Careful determi-

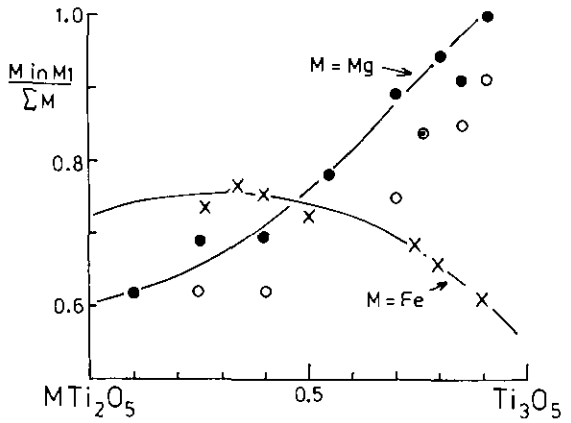

FIG. 4. Plots of the fraction of M in the $M1$ site vs x in $M_{1-x}Ti_{2+x}O_5$ obtained from constrained site occupancy refinements for M = Mg (circles) and from Mössbauer spectroscopy for M = Fe (crosses). Filled and open circles represent samples equilibrated close to the upper (M_3O_5 + MO_{2-x}) and lower (M_3O_5 + M_2O_3) phase boundaries, respectively. Results for M = Fe from Ref. (26).

nation of atomic charges from electron difference density studies on titanates (24) gives values in between fully ionised and neutral and the choice remains somewhat arbitrary.

In addition, the distribution of Mg and Ti between the two sites was found to be strongly dependent on the choice of atomic charges. Values of (Mg in $M1$)/ΣMg obtained were 0.51(1) for neutral atoms and 0.79(2) for fully ionized atoms. It was found that when the site occupancy refinements were constrained to maintain the [Mg]/[Mg + Ti] ratio at the bulk composition value (1/3 for $MgTi_2O_5$), then the refined distribution was essentially independent of the atomic charges used. Values of (Mg in $M1$)/ΣMg obtained were 0.60(1) and 0.62(1) for neutral and fully ionized atoms respectively. For comparison a value of 0.600(4) was obtained in a recent neutron powder diffraction study on a sample quenched from 1773 K (25). It was thus decided to proceed with this type of constrained refinement, using neutral atom scattering factors. Although the constraints imposed would give no direct information on cation site vacancies, it was anticipated that indirect evidence might be obtainable from thermal parameters and bond length–bond strength considerations.

The (Mg in $M1$)/ΣMg values obtained from the constrained refinements are presented as a function of x in Fig. 4. The results show that ordering of magnesium into the $M1$ site increases continuously with increasing x. This ordering is consistently lower for M_3O_5 solid solution phases equilibrated near the lower fO_2 phase boundary, shown by the open cireles in Fig. 4. The results are in contrast to those for the corresponding $Fe_{1-x}Ti_{2+x}O_5$ solid solution (26), plotted as crosses in Fig. 4, which show relatively constant Fe ordering in $M1$ over most of the composition range, with a decrease at higher x, in the monoclinic phases. The latter results were obtained by direct measurement of the relative peaks areas for Fe in $M1$ and $M2$ in the Mössbauer spectra (26). Based on the similar sizes and site preferences of Mg^{2+} and Fe^{2+}, and their reported parallel ordering behaviour in $Mg_{0.5}Fe_{0.5}Ti_2O_5$ (27), the ordering of Mg in $Mg_{1-x}Ti_{2+x}O_5$ would be expected to be qualitatively the same as for Fe in $Fe_{1-x}Ti_{2+x}O_5$. (Although see Ref. (8) for a counter example.) On this basis, the results shown in Fig. 4 are open to an alternative interpretation; that the observed increased ordering of the light scatterer Mg in $M1$ with increasing x is only apparent, and represents an attempt by the refinement to mimic the effect of increasing cation vacancies in $M1$ with increasing x.

To test the alternative interpretation, an algorithm was established for refinement of the cation site occupancies that maintained the [Mg]/[Mg + Ti] and (Mg in $M1$)/ΣMg ratios at constant values and maintained full occupancy of site $M2$, while allowing refinement of the occupancy of site $M1$. The [Mg]/[Mg + Ti] ratio was set to the bulk value, while the (Mg in $M1$)/ΣMg ratio followed the same change with x as reported for the corresponding $Fe_{1-x}Ti_{2+x}O_5$ system (26). From the refined site occupancies, the [O]/[M] ratio was calculated. The values are compared in Table 2 with experimental [O]/[M] ratios obtained by weight gain experiments. Because the scattering by metal atoms relative to oxygen atoms was varied in the refinement, the derived site occupancies are dependent on the values chosen for the atomic charges. In a few of the refinements the neutral atom scattering curves were replaced with those for fully ionized atoms, and the results are compared in Table 2. In comparison with the unconstrained refinements, the effect of ionization state was relatively small and it did not obscure the main results; that the [O]/[M] ratio obtained from the refinement is consistently higher than the stoichiometric value and that it has a maximum value in the vicinity of the orthorhombic-to-monoclinic transition. The closer agreement between the measured [O]/[M] ratios and the values derived from the refinements using neutral atoms may be fortuitous, but it is consistent with the near-neutral atomic charges obtained in single crystal studies of electron distributions in titanates (24). The generally good agreement between the measured and calculated [O]/[M] values lends support to the proposed model in which cation vacancies are confined to $M1$ sites and ordering of Mg between $M1$ and $M2$ has a similar dependence on x as in $Fe_{1-x}Ti_{2+x}O_5$.

Structure Results

In addition to providing information on nonstoichiometry as discussed above, Rietveld refinements were used

TABLE 2
Comparison of [O]/[M] Ratios Obtained from Weight Gain Experiments and Calculated from XRD Refinement Results

x in $Mg_{1-x}Ti_{2+x}O_5$	log fO_2	[O]/[M] from analyses	[O]/[M] from XRD refinements	
			Mg^0, Ti^0, O^0	Mg^{2+}, Ti^{4+}, O^{2-}
0.25	−14.5	1.680	1.693(4)	1.686(3)
0.25	−16.2	1.674	1.675(4)	1.667(3)
0.40	−14.5	1.684	1.690(4)	
0.40	−17.4		1.677(3)	
0.55	−15.0	1.688	1.702(4)	
0.60	−15.5	1.706	1.709(4)	1.695(5)
0.60	−18.2	1.691	1.694(4)	
0.85	−16.2	1.704	1.695(4)	
0.85	−18.5	1.684	1.693(4)	
0.91	−18.2	1.699	1.692(4)	1.671(4)

to study systematic trends in the M_3O_5 structures, particularly in relation to the change from orthorhombic to monoclinic symmetry as a function of composition. Results of the structure refinements using the Rietveld method on single phase products from the controlled atmosphere runs are summarised in Tables 3 and 4 for orthorhombic and monoclinic phases, respectively. For selected compositions, results are compared for phases prepared at fO_2

TABLE 3
Results of Structure Refinements for Orthorhombic $Mg_{1-x}Ti_{2+x}O_5$ Phases: Cell Parameters and Atomic Coordinates for Space Group *Ccmm*

	x						
	0.0	0.1	0.25	0.4	0.4	0.55	0.70
log fO_2	Air	−14.0	−14.5	−14.5	−17.2	−15.0	−16.2
R_{wp}	11.4	12.4	11.4	11.8	10.9	12.3	10.5
R_B	5.1	5.3	4.8	4.8	4.5	4.9	3.9
Goodness of fit	3.0	2.4	2.8	3.2	2.6	2.7	2.5
a	9.74926(5)	9.75557(9)	9.76470(9)	9.7753(1)	9.78360(9)	9.7894(1)	9.8070(1)
b	3.74650(2)	3.75230(3)	3.76178(3)	3.76851(4)	3.77211(3)	3.77516(5)	3.78029(4)
c	9.98563(6)	9.98684(9)	9.98855(9)	9.9864(1)	9.98000(9)	9.98361(1)	9.9774(1)
V	364.73	365.58	366.96	367.88	368.31	368.96	369.9
$M1$ (x 0 1/4)							
x	0.8074(1)	0.8069(1)	0.8064(1)	0.8060(1)	0.8063(1)	0.8059(1)	0.8054(1)
B	0.48(4)	0.35(4)	0.28(14)	0.42(4)	0.29(13)	0.34(4)	0.41(13)
$M2$ (x 0 z)							
x	0.1353(1)	0.1350(1)	0.1351(1)	0.1348(1)	0.1350(1)	0.1349(1)	0.1346(1)
z	0.0637(1)	0.0637(1)	0.0637(1)	0.0635(1)	0.0628(1)	0.0629(1)	0.0618(1)
B	0.58(2)	0.38(2)	0.33(2)	0.38(2)	0.34(2)	0.40(2)	0.41(3)
O1 (x 0 1/4)							
x	0.2305(4)	0.2287(5)	0.2289(4)	0.2300(5)	0.2325(4)	0.2309(5)	0.2331(4)
B	0.98(6)	0.68(7)	0.61(6)	0.63(7)	0.69(6)	0.60(7)	0.66(7)
O2 (x 0 z)							
x	0.0463(3)	0.0461(3)	0.0466(3)	0.0471(3)	0.0475(3)	0.0472(4)	0.0475(43)
z	0.8840(2)	0.8843(2)	0.8839(2)	0.8830(3)	0.8823(2)	0.8827(3)	0.8811(3)
B	0.89(5)	0.61(5)	0.68(5)	0.79(6)	0.60(5)	0.88(6)	0.77(6)
O3 (x 0 z)							
x	0.3114(3)	0.3118(3)	0.3122(3)	0.3120(3)	0.3117(3)	0.3122(3)	0.3129(3)
z	0.9313(2)	0.9312(3)	0.9321(3)	0.9319(3)	0.9309(3)	0.9318(3)	0.9316(3)
B	0.85(5)	0.66(5)	0.60(5)	0.67(5)	0.62(5)	0.60(5)	0.46(5)

TABLE 4
Results of Structure Refinements for Monoclinic $Mg_{1-x}Ti_{2+x}O_5$, Space Group $C2/m$

	x						
	0.76	0.85	0.85	0.91	0.94	1.0 (H)	1.0 (L)
$\log fO_2$	−16.2	−18.5	−16.2	−17.0	−16.7	−18.8	−18.8
R_{wp}	13.2	11.0	10.4	9.3	9.0	11.5	11.5
R_B	4.9	4.0	3.8	3.9	3.8	5.1	5.5
Goodness of fit	2.8	1.7	1.6	1.8	1.7	1.9	1.9
a	9.8143(2)	9.8230(1)	9.8284(3)	9.8307(2)	9.8285(1)	9.8261(2)	9.7568(2)
b	3.78290(6)	3.78434(6)	3.7820(1)	3.7837(1)	3.78632(6)	3.78937(9)	3.80077(9)
c	9.9746(2)	9.9696(1)	9.9741(3)	9.9700(3)	9.9694(1)	9.9694(2)	9.4389(1)
β	90.402(1)	90.831(1)	90.790(2)	91.011(1)	91.103(1)	91.258(2)	91.547(1)
V	370.31	370.56	370.70	370.79	370.92	371.12	349.90
$M1$ (x 0 z)							
x	0.8052(2)	0.8047(2)	0.8044(2)	0.8038(2)	0.8047(1)	0.8041(3)	0.7781(5)
z	0.2485(2)	0.2471(2)	0.2466(2)	0.2458(2)	0.2461(1)	0.2461(2)	0.2663(2)
B	0.30(5)	0.31(4)	0.19(5)	0.16(4)	0.40(2)	0.23(4)	0.10(4)
$M2$a (x 0 z)							
x	0.1341(2)	0.1323(1)	0.1323(2)	0.1310(2)	0.1310(1)	0.1301(3)	0.1276(5)
z	0.0592(2)	0.0555(1)	0.0561(2)	0.0547(2)	0.0533(1)	0.0529(2)	0.0437(2)
B	0.42(4)	0.41(4)	0.26(5)	0.45(4)	0.40(2)	0.52(4)	0.10(4)
$M2$b (x 0 z)							
x	0.1350(2)	0.1350(1)	0.1347(2)	0.1342(2)	0.1346(1)	0.1354(3)	0.0546(4)
z	0.4370(2)	0.4351(1)	0.4345(2)	0.4346(1)	0.4345(1)	0.4337(2)	0.3650(2)
B	0.29(4)	0.35(4)	0.22(4)	0.28(4)	0.28(2)	0.44(4)	0.10(4)
O1 (x 0 z)							
x	0.2348(6)	0.2366(6)	0.2336(6)	0.2336(6)	0.2362(5)	0.237(1)	0.233(2)
z	0.2520(1)	0.2502(6)	0.2508(8)	0.2507(6)	0.2505(5)	0.2506(9)	0.246(1)
B	0.57(9)	0.55(8)	0.4(1)	0.48(9)	0.5(1)	0.3(1)	0.64(7)
O2a (x 0 z)							
x	0.0476(8)	0.0469(7)	0.0467(9)	0.0467(7)	0.0471(6)	0.046(1)	0.051(2)
z	0.8767(7)	0.8744(5)	0.8782(7)	0.8752(6)	0.8727(5)	0.8736(8)	0.844(1)
B	0.7(1)	0.9(1)	0.9(1)	0.8(1)	0.8(1)	1.0(1)	0.64(7)
O2b (x 0 z)							
x	0.0491(7)	0.0502(6)	0.0543(8)	0.0532(7)	0.0517(6)	0.053(1)	0.130(2)
z	0.6170(7)	0.6158(6)	0.6149(8)	0.6129(6)	0.6150(5)	0.6116(8)	0.560(1)
B	0.6(1)	0.6(1)	0.4(1)	0.6(1)	0.4(1)	0.8(1)	0.64(7)
O3a (x 0 z)							
x	0.3177(7)	0.3180((6)	0.3184(8)	0.3183(7)	0.3186(6)	0.321(1)	0.328(2)
z	0.9324(6)	0.9319(5)	0.9312(7)	0.9321(6)	0.9326(5)	0.9368(8)	0.939(1)
B	0.0(1)	0.4(1)	0.0(2)	0.4(1)	0.3(1)	0.0(1)	0.64(7)
O3b (x 0 z)							
x	0.3108(8)	0.3101(6)	0.3144(8)	0.3116(7)	0.3098(6)	0.307(1)	0.408(2)
z	0.5719(8)	0.5720(6)	0.5716(7)	0.5731(6)	0.5729(5)	0.5740(8)	0.653(1)
B	0.9(2)	0.7(1)	0.4(2)	0.4(1)	0.4(1)	0.7(1)	0.64(7)

values close to both the upper and lower phase boundaries. With the lowering of the space group symmetry from Ccmm in the orthorhombic phases to $C2/m$ in the monoclinic phases the eightfold sites $M2$, O2, and O3 each split into pairs of fourfold sites. To maintain the obvious relationship between the two situations, these sites are labeled $M2$a, $M2$b, O2a, O2b, and O3a, O3b in Table 4. A typical Rietveld plot, for the monoclinic phase $Mg_{0.05}Ti_{2.95}O_5$, is shown in Fig. 5.

Plots of the cell parameters and cell volume vs x for single-phase M_3O_5 compositions are given in Fig. 6. The solid solution involves the progressive substitution of $2Ti^{3+}$ for $(Mg^{2+} + Ti^{4+})$. The average ionic radii are similar, 0.67 and 0.66 Å, respectively, and this is reflected in the small unit cell volume change of 1.75% over the full composition range. The changes to the individual cell parameters are anisotropic; a and b increase while c decreases with increasing x. The cell parameters obtained by

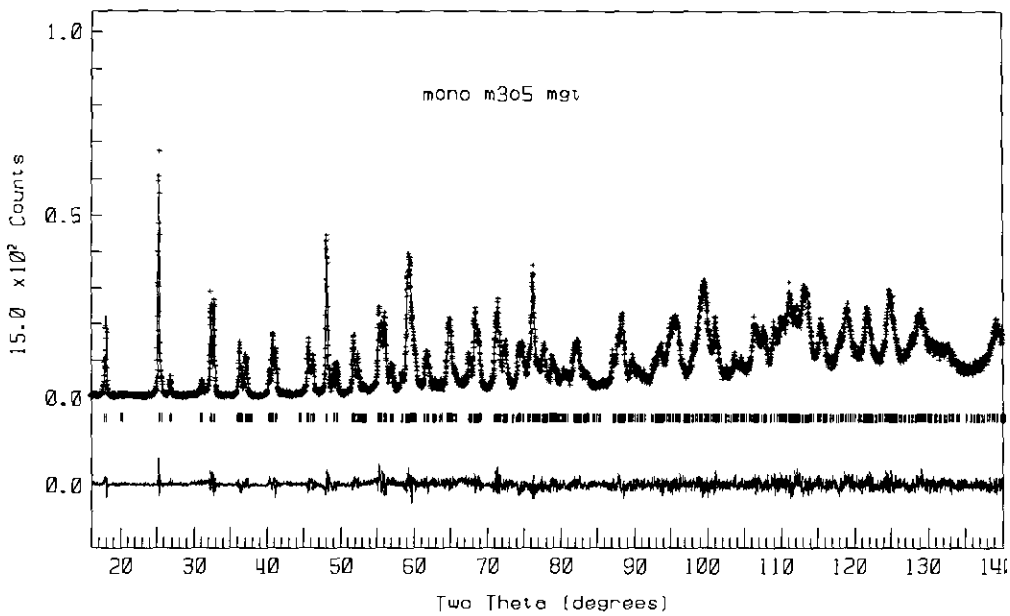

FIG. 5. Observed, calculated, and difference X-ray powder diffraction profiles for $Mg_{0.05}Ti_{2.95}O_5$, equilibrated at $fO_2 = 10^{-16.2}$ atm. The observed data (variable time data collection) are indicated by crosses and the calculated profile by the continuous line. Positions of Bragg reflections are shown by tick marks, and below them is the profile corresponding to the difference between the observed and calculated patterns.

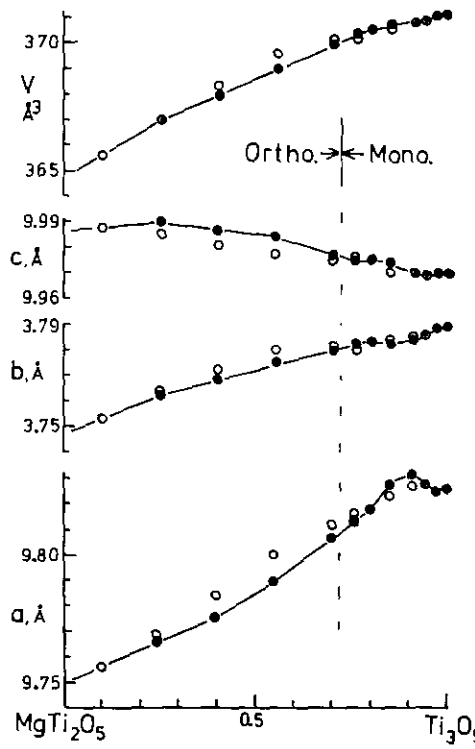

FIG. 6. Variation of cell parameters and unit cell volume as a function of x in $Mg_{1-x}Ti_{2+x}O_5$. Filled and open circles represent samples equilibrated close to the upper ($M_3O_5 + MO_{2-x}$) and lower ($M_3O_5 + M_2O_3$) phase boundaries, respectively.

Rietveld refinement have high relative precision, allowing fine detail to be discerned in the relationships between cell parameters and composition. The filled circles in Fig. 6 correspond to samples equilibrated close to the $M_3O_5 + MO_{2-x}$ phase boundary, where the nonstoichiometry is greatest, while the open circles correspond to samples equilibrated close to the $M_3O_5 + M_2O_3$ phase boundary. Smooth curves have been drawn through the filled circles. For $0.25 < x < 0.7$ (orthorhombic phases), the open circles (lower fO_2) are consistently displaced from the curves such that a, b, and V are higher, while c is lower than for corresponding samples equilibrated at higher fO_2's. The direction of change of the cell parameters and volume with increasing fO_2 is the same as that observed for the parameters of $MgTi_2O_5$ and $Mg_{0.5}Fe_{0.5}Ti_2O_5$ when they are quenched from progressively lower temperatures (25, 27). In these latter cases the observed parameter changes correspond to an increase in the size of the $M1$ octahedral site (increased ordering of Mg, Fe into $M1$). An expansion of the $M1$ site is also expected to result from increasing the vacancy content of this site (28). For $x > 0.7$ (monoclinic phases) the effect of fO_2 on the lattice parameters is significantly smaller and less well defined than for the orthorhombic phases.

The average $M1$–O and $M2$–O bond lengths in the $Mg_{1-x}Ti_{2+x}O_5$ phases, obtained from the Rietveld refinement results, are plotted as a function of x in Fig. 7. The general trends are a decrease in $\langle M1\text{–O}\rangle$ and an increase in $\langle M2\text{–O}\rangle$ with increasing x. For the monoclinic phases, $M2$ splits into $M2$a and $M2$b, and there is a diver-

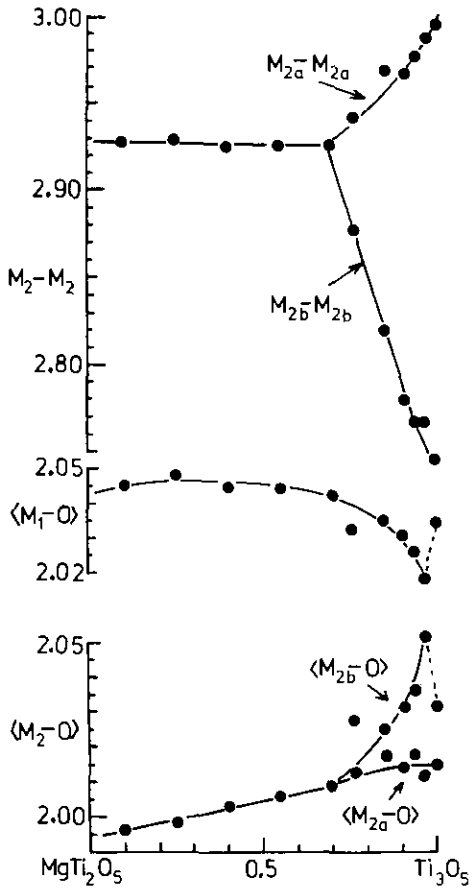

FIG. 7. Average ⟨*M*1–O⟩, ⟨*M*2–O⟩, and shortest *M*2–*M*2 distances as a function of x in $Mg_{1-x}Ti_{2+x}O_5$.

gence of the ⟨*M*2a–O⟩ and ⟨*M*2b–O⟩ average bond lengths. The ⟨*M*2a–O⟩ remain relatively constant while the ⟨*M*2b–O⟩ values increase steeply with increasing x up to $x = 0.97$. At $x = 0.97$, the calculated valences for *M*1, *M*2a, and *M*2b from bond length–bond strength calculations (29) are 3.42, 3.46, and 3.18, respectively, corresponding to partial ordering of Ti^{3+} into the *M*2b site. For $x = 1.0$ (high-Ti_3O_5) the corresponding values are 3.23, 3.45, and 3.41, respectively, closer to a random distribution of T^{3+} and Ti^{4+}. The change in distribution for high-Ti_3O_5 is reflected in the reversal of the ⟨*M*–O⟩ trends at $x = 1$ in Fig. 7. This may be partly an artifact of the refinement, which was for a two-phase mixture of high- and low-Ti_3O_5 for the end-member composition. The ⟨Ti1–O⟩, ⟨Ti2a–O⟩ and ⟨Ti2b–O⟩ distances for low-Ti_3O_5 obtained from the two-phase refinements were 1.989, 2.016, and 2.053 Å, respectively, more in line with the trends for $Mg_{1-x}Ti_{2+x}O_5$, and giving calculated valences of 3.75, 3.46, and 3.06, respectively.

Figure 7 also shows the variation of the shortest *M*2–*M*2 separation as a function of x. This distance is essentially constant in the orthorhombic phases. In the monoclinic phases the *M*2a–*M*2a and *M*2b–*M*2b distances diverge sharply; *M*2a–*M*2a increases while *M*2b–*M*2b shows a pronounced decrease with increasing x, from 2.923(2) Å at $x = 0.7$ to 2.744(6) Å at $x = 1$ (high-Ti_3O_5). This distance decreases further, to 2.608(9) Å in low-Ti_3O_5. The decrease in *M*2b–*M*2b due to increasing Ti^{3+}–Ti^{3+} bonding is by far the major structural change in the monoclinic phases and is clearly the driving force for the lowering of symmetry at $x = 0.72$. Studies on electronic conductivity indicate that local Ti^{3+}–Ti^{3+} pairing begins in the orthorhombic phases, between $x = 0.5$ and $x = 0.7$ (9).

A useful way to view the structural changes in the M_3O_5 solid solution is the polyhedral approach (30). Following Swanson and Peterson (31), octahedral volumes for *M*1 and *M*2 have been calculated by summing the volumes of the eight $MO_aO_bO_c$ segments comprising the octahedra. The variance of the eight segment volumes, σ_v has been used as a measure of the distortions of the octahedra. $\sigma_v = \Sigma(V_i - V_0)^2/(n - 1)$ where V_0 is the volume of an octant of an undistorted octahedron having a bond length equal to ⟨*M*1–O⟩ or ⟨*M*2–O⟩. The results are given in Table 5. The individual octahedral volumes are summed to give the octahedral volume per unit cell, and this has been subtracted from the cell volume to give a measure of the total interstitial volume per unit cell in Table 5.

From Table 5 it is seen that the $M1O_6$ octahedron is considerably more distorted than the $M2O_6$ octahedron in the orthorhombic solid solution members, but they become comparable in the monoclinic phases due to a large increase in the distortion of $M2aO_6$ and $M2bO_6$ and a decrease in the distortion of $M1O_6$. With increasing x there is a progressive increase in the volumes of both $M1O_6$ and $M2O_6$, although the relative increase is much greater for the latter. The effect of increase of fO_2 at fixed x is to decrease the size of $M2O_6$ and increase the size of $M1O_6$. This may be due to an increasing vacancy concentration in *M*1 with a corresponding increase in Ti^{4+} in *M*2, but increasing ordering of Mg^{2+} into *M*1 with increasing fO_2 would also explain the observed changes. The increase in the $M1O_6$ volume with increase of fO_2 was not observed for the $x = 0.7$ composition. This is at the limit of the orthorhombic series, and strong local Ti^{3+}–Ti^{3+} bonding may be contributing to the difference.

Table 5 shows that significant polyhedral changes accompany the high- to low-Ti_3O_5 transformation. There is a large increase in $M2aO_6$ and $M2bO_6$ volumes due both to increased Ti^{3+} ordering from *M*1 into these sites and to a marked decrease in the distortion of the $M2aO_6$ and $M2bO_6$ octahedra. The large decrease in volume accompanying the transformation is seen to result exclusively from

TABLE 5
Polyhedral Volumes (Å^3) and Distortions in $Mg_{1-x}Ti_{2+x}O_5$

		Octahedral volume (O.V.) (Å^3)					Distortion index $\Sigma(V - V_0)^2/n - 1$		
x	log fO_2	$M1$	$M2$		ΣO.V.	Interstitial volume	$M1$	$M2$	
0.0	Air	10.12	10.05		120.85	243.85	0.028	0.017	
0.4	−14.5	10.23	10.16		122.16	245.72	0.027	0.017	
0.4	−17.4	10.16	10.23		122.51	245.80	0.024	0.017	
0.7	−16.2	10.23	10.34		123.6	246.3	0.024	0.015	
0.7	−18.2	10.25	10.38		124.1	246.1	0.025	0.016	
			$M2$a	$M2$b				$M2$a	$M2$b
0.85	−16.2	10.28	10.36	10.60	125.0	245.7	0.021	0.018	0.022
0.85	−18.5	10.14	10.36	10.74	124.7	245.8	0.020	0.019	0.020
1.0 (H)	−18.8	10.22	10.15	10.76	124.5	246.6	0.021	0.022	0.024
1.0 (L)	−18.8	10.14	10.60	11.16	127.6	222.3	0.015	0.012	0.008

a decrease in the interstitial volume (the total polyhedral volume actually increases). The ratio of interstitial to octahedral volume is in a relatively narrow range of 1.97–2.02 over the complete solid solution, whereas for low-Ti_3O_5, in which the anion packing approximates to face-centered cubic close packing, this ratio drops to 1.74.

CONCLUSIONS

The $Mg_{1-x}Ti_{2+x}O_5$ solid solution is complete at 1473 K. Members of the solid solution series have orthorhombic symmetry for $x < 0.72$ and monoclinic symmetry for high x values. From structure refinements on the solid solution members, the origin of the symmetry lowering has been shown to be cooperative metal–metal bonding in the $M2$ sites. In the monoclinic phases the eightfold $M2$ sites split into two fourfold sites and the M–M bonding is confined to one of these sites, $M2$b. The $M2$b–M2b distance decreases from 2.92 to 2.74 Å as x increases from 0.7 to 1.0.

The M_3O_5 phases prepared in H_2/H_2O and H_2/CO_2 gas mixtures at 1473 K are nonstoichiometric, with [O]/[M] ratios higher than the stoichiometric value of 5/3 = 1.667. The nonstoichiometry goes through a broad maximum, with [O]/[M] = 1.705, at compositions close to the orthorhombic to monoclinic transition. The nonstoichiometry range of Ti_3O_5 was also determined at 1323 K, using interpellet oxygen transport in a sealed evacuated silica tube. The deviation in [O]/[Ti] is only ~0.001 under these conditions.

Constrained refinement of site occupancies gave preferential ordering of Mg into $M1$, with (Mg in $M1$)/ΣMg = 0.6 at $x = 0$, and progressively increasing to a fully ordered value of 1 at higher x values. An alternative interpretation of the results is that the *apparent* Mg ordering obtained in the refinements is compensating for ordering of cation vacancies in $M1$. On this basis, and assuming the Mg ordering has the same dependency on x as for the corresponding $Fe_{1-x}Ti_{2+x}O_5$ solid solution, site occupancy refinements led to calculated values of [O]/[M] that agree reasonably well with the experimental values obtained from analyses. However, an unambiguous resolution of the magnesium and vacancy ordering requires further study. We have recently undertaken a neutron diffraction study to help resolve the ambiguity. Preliminary results support the ordering of cation vacancies in site $M1$, as found in an earlier study (8).

REFERENCES

1. L. Pauling, *Z. Kristallogr.* **73,** 97 (1930).
2. N. A. Vasyutinskii and A. P. Sidorenko, *Sb. Tr. Nauchno-Issled. Proektn. Inst. Titana* **5,** 22 (1970).
3. J. Barksdale, "Titanium. Its Occurrence, Chemistry and Technology," second ed. Ronald Press, New York, 1966.
4. I. D. Martin and H. W. Hockin, U.S. Patent 3,502,460 (1970).
5. J. K. Tuset, *Tidsskr. Kjemi Bergves. Metall.* **28,** 232 (1968).
6. K. Borowiec and T. Rosenqvist, *Scand. J. Metall.* **14,** 33 (1985).
7. S. Asbrink and A. Magneli, *Acta Crystallogr.* **12,** 575 (1959).
8. R. G. Teller, M. R. Antonio, A. E. Grau, M. Gueguin, and E. Kostiner, *J. Solid State Chem.* **88,** 334 (1990).
9. M. Steinbruck and A. Feltz, *Z. Anorg. Allg. Chem.* **594,** 157 (1991).
10. I. E. Grey, C. Li, and A. F. Reid, *J. Solid State Chem.* **17,** 343 (1976).
11. I. E. Grey and R. R. Merritt, *J. Solid State Chem.* **37,** 284 (1981).
12. I. E. Grey, C. Li, and A. F. Reid, *J. Solid State Chem.* **11,** 120 (1974).
13. I. C. Madsen and R. J. Hill, *Adv. X-Ray Anal.* **35,** 39 (1992).
14. R. J. Hill and C. J. Howard, *J. Appl. Crystallogr.* **18,** 173 (1985).
15. D. B. Wiles and R. A. Young, *J. Appl. Crystallogr.* **14,** 149 (1981).
16. G. Caglioti, A. Paoletti, and F. P. Ricci, *Nucl. Instrum.* **3,** 223 (1958).
17. R. J. Hill and I. C. Madsen, *J. Electrochem. Soc.* **131,** 1486 (1984).
18. "International Tables for X-Ray Crystallography," Vol. IV. Kynoch Press, Birmingham 1974.
19. A. Magneli, S. Andersson, L. Kihlborg, S. Asbrink, S. Westman,

B. Holmberg, and C. Nordmark, "Studies on the Crystal Chemistry of Titanium, Vanadium and Molybdenum Oxides at Elevated Temperatures." Final Technical Report No. 1, University of Stockholm, Oct. 1959.
20. W. A. Dollase, *J. Appl. Crystallogr.* **19,** 267 (1986).
21. A. B. Sheikh and J. T. S. Irvine, *J. Solid State Chem.* **103,** 30 (1993).
22. C. N. R. Rao, S. Ramdas, R. E. Loehman, and J. M. Honig, *J. Solid State Chem.* **3,** 83 (1971).
23. I. E. Grey, *in* "Proceedings of Third European Powder Diffraction Conference, EPDIC-3, Vienna, September 1993."
24. R. H. Buttner and E. N. Maslen, *Acta Crystallogr. Sect. B* **48,** 644 (1992).
25. B. A. Wechsler and R. B. von Dreele, *Acta Crystallogr. Sect. B* **45,** 542 (1989).
26. I. E. Grey and J. Ward, *J. Solid State Chem.*, **7,** 300 (1973).
27. B. A. Weschler, *Am. Mineral.* **62,** 913 (1977).
28. R. J. Hill, *Acta Crystallogr. Sect. B* **37,** 1323 (1981).
29. W. H. Zachariasen, *J. Less-Common Met.* **62,** 1 (1978).
30. R. H. Hazen, *Am. J. Sci.* **288A,** 242 (1988).
31. D. K. Swanson and R. C. Peterson, *Can. Mineral.* **18,** 153 (1980).